

PAPER • OPEN ACCESS

The influence of laser etching biomimicking configuration on the strength of metal-plastic connection

To cite this article: Fengde Liu *et al* 2022 *Mater. Res. Express* **9** 056520

View the [article online](#) for updates and enhancements.

You may also like

- [Design methodologies and engineering applications for ecosystem biomimicry: an interdisciplinary review spanning cyber, physical, and cyber-physical systems](#)
Kathryn Hinkelman, Yizhi Yang and Wangda Zuo
- [Biomimicked large-area anisotropic grooves from *Dracaena sanderiana* leaf enhances cellular alignment and subsequent differentiation](#)
Shital Yadav and Abhijit Majumder
- [Biomimicking interfacial fracture behavior of lizard tail autotomy with soft microinterlocking structures](#)
Navajit S Baban, Ajymurat Orozaliev, Christopher J Stubbs *et al.*



244th Electrochemical Society Meeting

October 8 – 12, 2023 • Gothenburg, Sweden

50 symposia in electrochemistry & solid state science

Abstract submission deadline:
April 7, 2023

Read the call for
papers &
submit your abstract!

Materials Research Express



PAPER

OPEN ACCESS

RECEIVED
8 February 2022

REVISED
27 April 2022

ACCEPTED FOR PUBLICATION
9 May 2022

PUBLISHED
25 May 2022

Original content from this work may be used under the terms of the [Creative Commons Attribution 4.0 licence](#).

Any further distribution of this work must maintain attribution to the author(s) and the title of the work, journal citation and DOI.



The influence of laser etching biomimicking configuration on the strength of metal-plastic connection

Fengde Liu^{1,2,*}, Xiaoni Xu^{1,2}, Jiaming Liu¹, Haiqi Fan^{1,2,3}, Genzhe Huang^{1,2} and Hong Zhang^{1,2}

¹ College of Mechanical and Electric Engineering, Changchun University of Science and Technology, Changchun 130022, People's Republic of China

² National Base of International Science and Technology Cooperation in Optics, Changchun 130022, People's Republic of China

³ Changchun Institute of Optics, Fine Mechanics and Physics, Chinese Academy of Sciences, Changchun 133033, People's Republic of China

* Author to whom any correspondence should be addressed.

E-mail: lfid@cust.edu.cn

Keywords: laser prepared bionic configuration, stainless steel and plastic, connection strength, simulation

Abstract

This study uses a laser to etch biomimicking locking patterns on the surface of 304 stainless steel to strengthen the connection between metal-plastic products. Under heat and pressure from the device, the plastic melts into the pattern and coalesces it, while the burrs formed from the etching process lock the joint of the metal-plastic. Three biomimicking configurations, honeycomb, leaf vein, and dragonfly head-and-neck hair interlocking, are studied. As shear strength determines the connection strength, we simulate the tensile-shearing process of stainless steel and plastic connectors of the three biomimicking configurations on ABAQUS, and predict the effects of the configurations on their connection strength. Experiments show that the plastic and metal are effectively connected at a heating temperature of 400 °C and a pressure of 70 kN. When the burr rate is 7.66% and the coverage rate is $29.4 \pm 0.5\%$, the three biomimicking connectors break at the plastic base material, and the dragonfly head-and-neck hair interlocking configuration can withstand a shear force of 942 ± 9.23 N.

1. Introduction

The metal-plastic connection between two welded objects offers fatigue resistance, corrosion resistance, and less weight. Its composite form is widely used in automobiles, electronics, medicine, and aerospace [1–5]. The major metal-plastic connection methods are adhesive connection, mechanical connection, hybrid connection, and special configuration connection [6–10]. The adhesive connection method requires a certain curing time. The adhesive used therein is volatile. It is also susceptible to environmental stressors and pollutes the environment. The mechanical connection method requires positioning and perforation, which causes stress concentration, and low production efficiency, and affects the service life of the material. This study proposes a method of laser-processing biomimicking configurations, honeycombs, leaf veins, and dragonfly head-and-neck microhairs, into the metal surface, where the plastic is heated and pressurized to bond with the laser-etched locking patterns in the metal. Under heat and pressure from the device, the molten plastic penetrates the biomimicking configuration on the metal surface, causing the connector to form a mechanical linkage [11].

High roughness and porosity can improve the connection strength between metal and plastic. A few studies have proposed surface treatment methods such as sandblasting, shot blasting, chemical treatment, and micromilling [12–15]. However, these methods have low flexibility and high toxicity. To resolve these problems, studies have used lasers to treat metal surfaces [16, 17]. Zhang X [18] first adopted the method of laser processing to treat ceramic surfaces and form conical microstructures. They further processed the sand-pattern microstructure on the surface of an alloy steel. Next, they used an adhesive to join the ceramic and metal. The laser-processed parts were stronger than those processed with simple mechanical treatments. Xu F [19] designed

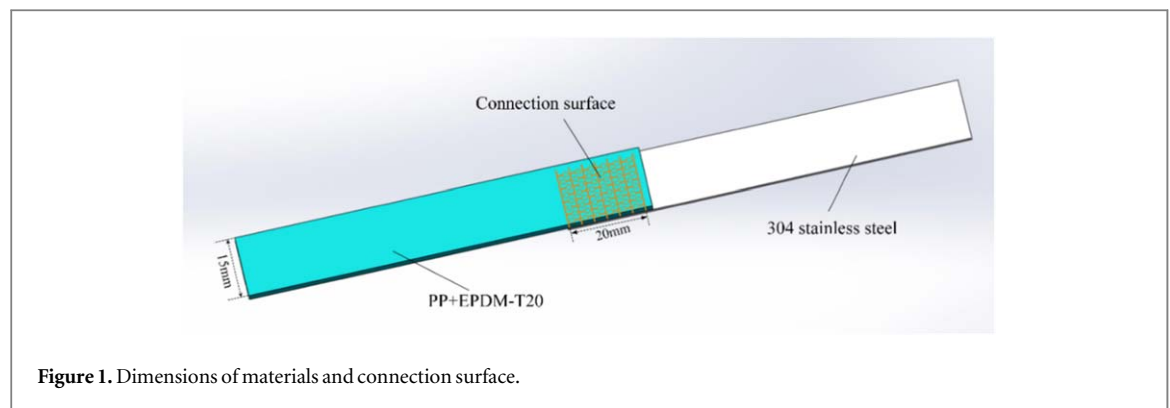


Figure 1. Dimensions of materials and connection surface.

Table 1. Physical properties of 304 stainless steel and PP + EPDM-T20.

Materials	Density	Elastic modulus	Fusion point	Tensile strength
304 stainless steel	7.93 g cm^{-3}	194,020 MPa	1398 °C–1454 °C	$\geq 520 \text{ MPa}$
PP + EPDM-T20	$1.05 \pm 0.02 \text{ g cm}^{-3}$	$\geq 1900 \text{ MPa}$	160 °C	$\geq 20 \text{ MPa}$

a circular array structure on the surface of stainless steel and used heat and pressure to infuse the melted plastic into the microstructure. He found that the surface was better connected with the plastic after laser treatment, and that the connection strength was related to factors including the micropore diameter. Fan H [20] laser-processed the circular array configuration on the surface of 304 stainless steel and bonded it to plastic under heat and pressure. The influences of temperature, connection pressure, coverage rate, and other factors on the connection strength between the two materials were studied, and the concept of ‘burr rate’ was introduced. Through tensile experiments, they discovered that the burr height, burr rate, and coverage rate, within a certain range, significantly improved the connection strength of stainless steel and plastic. Xing Y [21] used optimized laser-processing parameters to develop a microchannel with a depth of 40–45 μm and a width of 55–60 μm , which resulted in a biomimicking configuration on the ceramic surface with sound performance and produced microtextures that emulated animal features. Studies have demonstrated the possibility of solving certain engineering problems with biomimicry-based surface treatment methods. However, few have investigated the connection technology of dissimilar materials based on such surfaces or specific surface configurations.

This study constructed three biomimicking configurations, honeycomb, leaf vein, and dragonfly head-and-neck microhairs, on the metal end of 304 stainless steel to increase the surface contact area between the metal and the plastic under heat and pressure. Consequently, the burr distribution after laser processing on the microstructured surface and the strength of the connection between metal and plastic increased remarkably. ABAQUS was used to simulate the tensile and shearing processes of stainless steel and plastic to predict their connection strength. The laser-processed biomimicking configurations and the relationship between the strength of the metal–plastic connection was obtained according to a practical tension and shearing test.

2. Test materials and methods

For the test, we used 304 stainless steel and automotive polypropylene/EPDM rubber (PP + EPDM-T20) as the metal and plastic surfaces, respectively. The physical and mechanical properties of these materials are listed in table 1. The dimensions of the 304 stainless steel and PP + EPDM-T20 samples were 15 mm \times 100 mm \times 1 mm and 15 mm \times 100 mm \times 2.5 mm, respectively. A fiber laser (IPG fiber laser; model YLPM-1–4 \times 200–20–20) was used to etch the biomimicking configuration of the connection area on the steel surface. The connection area between the two materials was 15 \times 20 mm² (figure 1).

The IPG fiber laser of model YLPM-1–4 \times 200–20–20 was used in the test, its parameters are summarized in table 2. EzCAD was used to control the laser-scanning parameters, so that the beam scanned within the designed biomimicking configuration pattern. An appropriate focal length should be selected for laser processing; too large or too small of a focal length would result in insufficient laser energy and alter the surface texture quality. The focal length in this study was 265 mm, and the spot diameter was 0.05 mm. In the configuration unit, taking the honeycomb configuration as an example (figure 2), the laser beam scanned in the X direction, and then in the Y direction from +Y to -Y. After the laser processing of the stainless-steel surface, the biomimicking texture

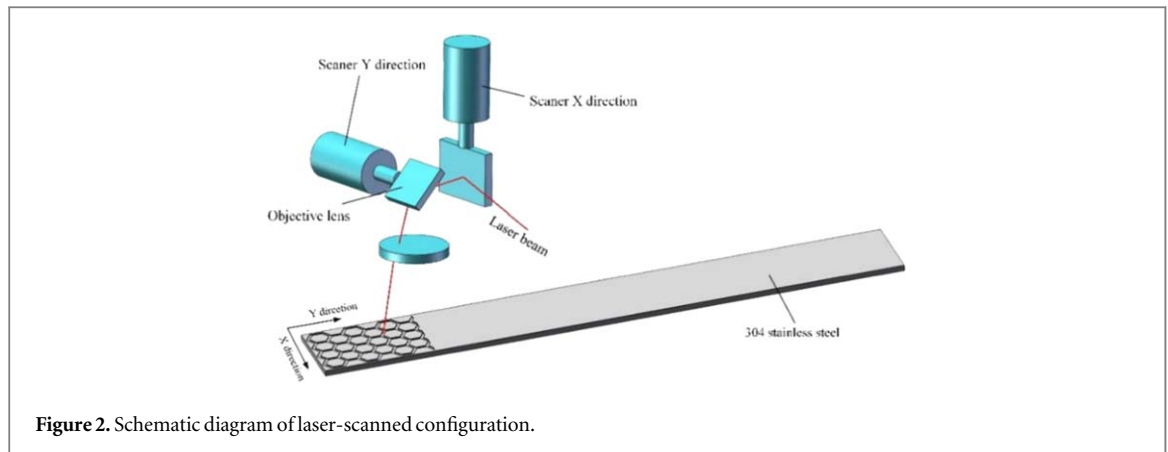


Figure 2. Schematic diagram of laser-scanned configuration.

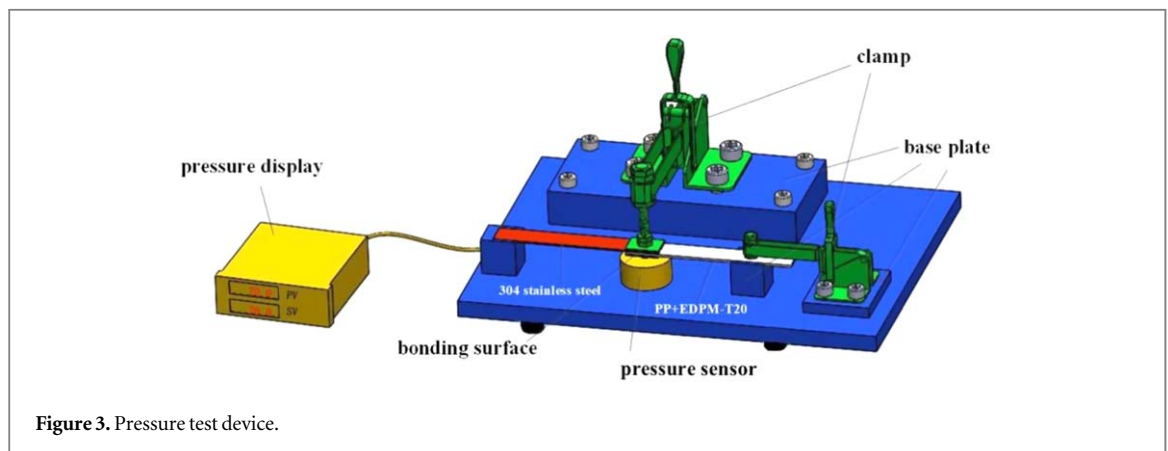


Figure 3. Pressure test device.

Table 2. Parameters of the laser equipment.

Parameters	Values	Parameters	Values
Wavelength	1064 nm	Average power	20W
Pulse duration	100 μ s	Frequency	20 kHz
Pulse energy	1 mJ	Spot diameter	$\varnothing 0.05$ mm
Power density	510 mW cm ⁻²	Functional range	100 mm \times 100 mm
Scanning speed	1000 mm s ⁻¹	Focal distance	265 mm

increased the contact area between the metal and the plastic, and the burrs in the biomimicking texture increased the connection strength between the metal and the plastic.

The coverage rate at a heating temperature of 400 °C and a compressive force of 70 kN was $29.4 \pm 0.5\%$. The test was performed to study the connection strength of 304 stainless steel and plastic when the burr rates of the three biomimicking configurations were 5.81% and 7.66%, respectively. During the test, the biomimicking configurations were first scanned on the surface of the steel with a laser, and then heated to the required temperature in an electric furnace. Next, the steel plate was withdrawn and fixed to the fixed plastic plate on the pressure connection device, A tightening mechanism was employed to tighten the connection of the two materials. Figure 3 illustrates the pressure device. During the joining process, the heated stainless-steel plate transfers heat to the plastic plate, which partially melts the plastic surface. The melted plastic flows into the biomimicking configuration of the stainless-steel surface under the action of pressure. The pressure was sustained for 1 min to ensure an effective connection between the 304 stainless steel and the plastic. After the two materials were connected, the connection strength of the connecting parts was tested by a 150DX hydraulic test universal testing machine (Instron, US) at 2 mm min⁻¹. To ensure a uniform force on the connector, pads of corresponding thicknesses were installed at both ends of the different materials when clamping the connector

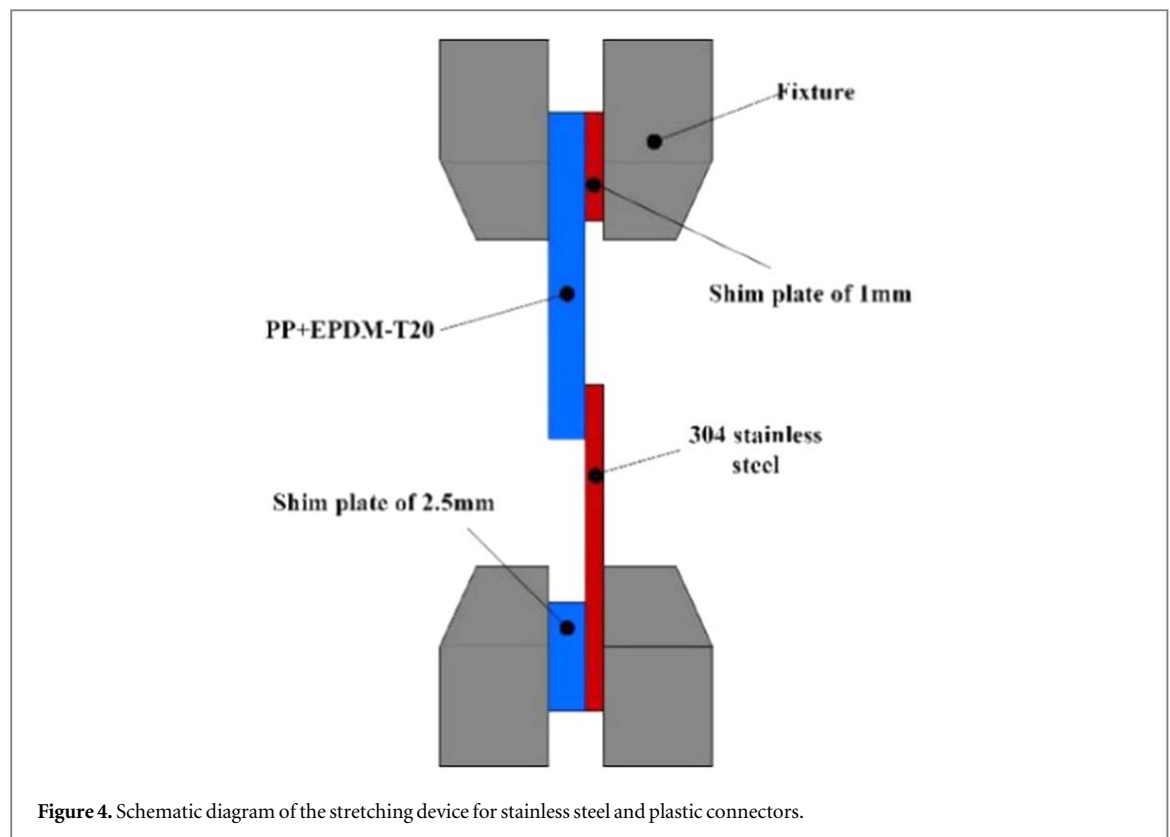

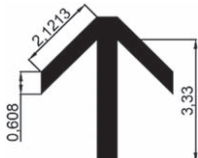
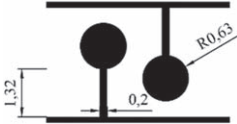


Figure 4. Schematic diagram of the stretching device for stainless steel and plastic connectors.

Table 3. Configuration design parameters.

Configuration	One unit size	Total area (mm ²)	Coverage rate(%)
Honeycomb		88.478	29.49
Vein		87.73	29.24
Interlock		86.53	28.84

(figure 4). Scanning electron microscopy (SEM; EVOMA25, Zeiss, Germany) was used to observe the microstructure of the connection between the metal and the plastic. A laser scanning confocal microscope (LSM700, Zeiss, Germany) was used to observe the biomimicking configuration on the stainless-steel surface.

3. Biomimicking configuration design and definition of experimental physical quantities

The total area of the biomimicking configuration of the laser-structured stainless-steel surface is $15 \times 20 \text{ mm}^2$. To ensure the unity of all parameters of the three biomimicking configurations except the configuration. We introduce a formula for coverage rate:

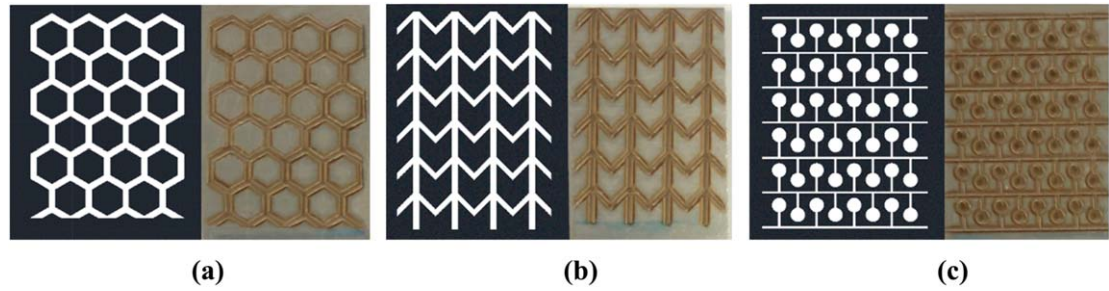


Figure 5. Three types of biomimicking configuration design drawings. (a) honeycomb configuration; (b) leaf vein configuration; (c) dragonfly head-and-neck hairs interlocking configurations.

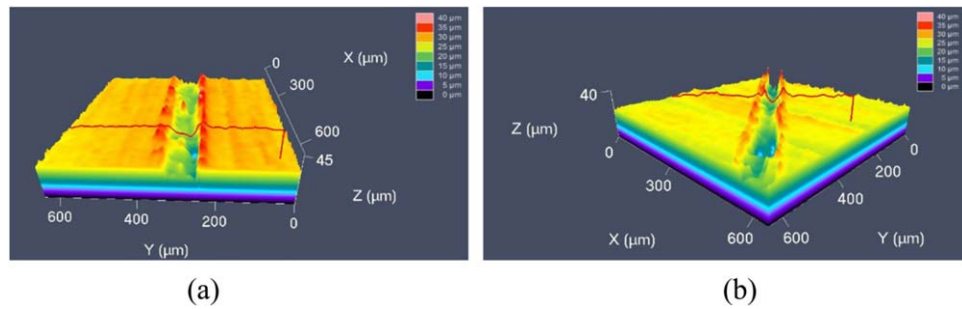


Figure 6. Surface morphology of stainless steel with a spot diameter of 0.5 mm. (a) laser marking conducted twice, $\lambda = 5.81\%$; (b) laser marking conducted five times, $\lambda = 7.66\%$.

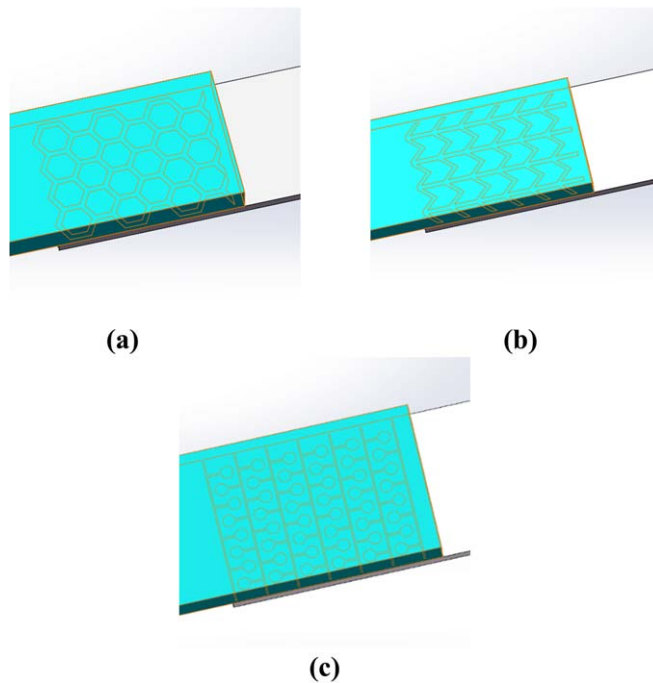


Figure 7. Geometric model of the lap joint after simplification of the three types of biomimicking configurations. (a) honeycomb; (b) leaf vein; (c) dragonfly head-and-neck hairs interlocking configurations.

$$\beta = \frac{S_u}{S} \quad (1)$$

where β is the coverage rate, S_u is the area of biomimicking configuration, and S is the area of the lap coincidence area ($15 \times 20 \text{ mm}^2$). The design parameters of the biomimicking configuration of a single unit are listed in

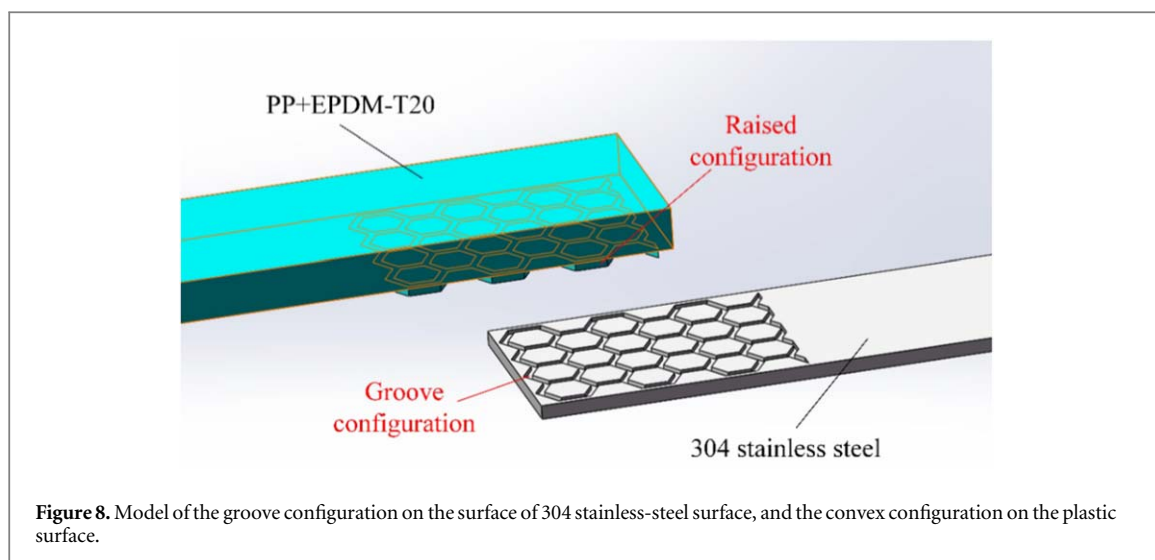


Figure 8. Model of the groove configuration on the surface of 304 stainless-steel surface, and the convex configuration on the plastic surface.

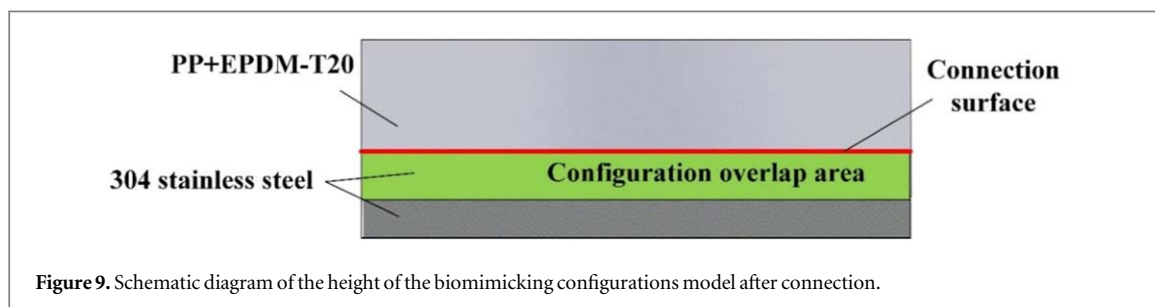


Figure 9. Schematic diagram of the height of the biomimicking configurations model after connection.

table 3. The coverage of the three biomimicking configurations is $\beta = 29.4 \pm 0.5\%$. Figure 5 illustrates the design and the corresponding physical forms of the three biomimicking configurations in the overlapping area.

Several high and low burrs appeared on the stainless-steel surface after laser treatment. Next, we assumed the stainless-steel surface as the reference plane. We obtained the total number of burrs in the configuration and the number of burrs with a height of 10–20 μm , according to data obtained after processing with the laser confocal microscope. Further, we introduced the proportion (λ) of the number of 10–20- μm -high burrs accounting for the total number of burrs. This proportion is expressed as follows:

$$\lambda = \frac{q}{m} \quad (2)$$

where λ is the burr rate, q is the quantity of burrs in the 10–20 μm height range, and m represents the total quantity of burrs in the biomimicking configuration region.

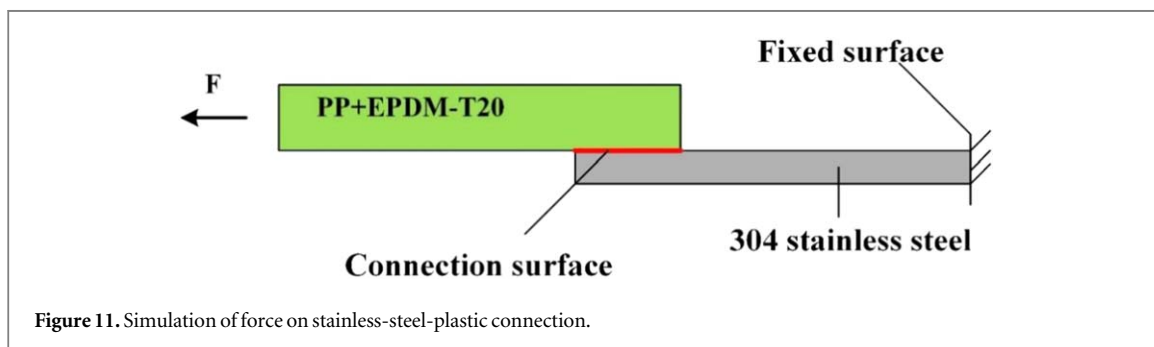
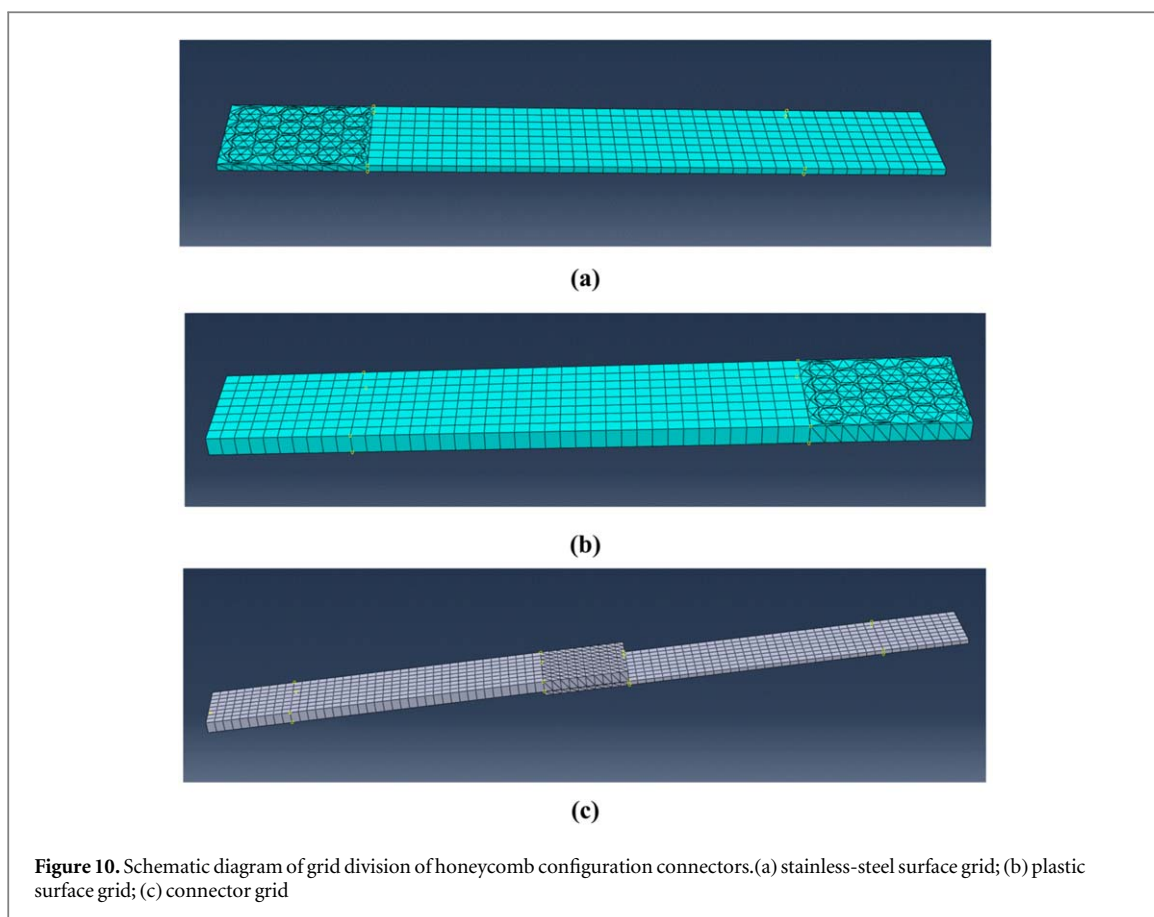
Figure 6 illustrates the local three-dimensional topography of the metal surface after laser etching the biomimicking configuration, for a varying, number of laser etchings is different and a constant spot diameter of 0.5 mm. We used λ to represent the burr rate in the range of 10–20 μm height. According to the different laser marking times, $\lambda = 5.81\%$ and $\lambda = 7.66\%$ were selected as the process parameters of biomimicking configuration etching to treat the stainless-steel surface.

4. Simulation of tensile shear test of metal-plastic connector

ABAQUS was used to simulate the tensile shear process of the stainless-steel and plastic connectors with the honeycomb, leaf veins and dragonfly head-and-neck microhair interlocking configurations. Subsequently, the influences of the three biomimicking configurations on the connection strength were analyzed and predicted.

4.1. Construction of the finite element model of the biomimicking configuration connector

Solidworks was used to construct geometric models of the three biomimicking configurations (figure 7). The process of tensile test involves several uncontrollable variables. This study only examines the influence of the configurations on the connection strength of stainless-steel and plastic, therefore, the actual connection process



was enlarged and simplified. After undergoing heating and pressing, molten plastic flows into the grooves on the stainless-steel surface, which is simplified into a raised configuration at the connecting surface. We take the honeycomb configuration as an example. The groove configuration on the 304 stainless-steel surface can be tightly integrated with the convex configuration on the plastic surface (figure 8). A friction force was imposed on the connecting surface to replace the effect of the burr, and simulate the stretching process of the stainless-steel and plastic connector.

The simplified height of the biomimicking configuration is the sum of the depth generated during the laser processing and the height of the highest burr. A simplified schematic diagram of the connector is depicted in figure 9. The simulated burr rate λ was 5.81%, the number of laser-marking iterations was 2, the depth of the stainless-steel surface configuration after laser treatment was $22.34 \mu\text{m}$, and the height of the highest burr was $18.16 \mu\text{m}$, i.e., the height of the configuration was $40.50 \mu\text{m}$.

4.2. Finite element model meshing

After constructing the model, we used ABAQUS for meshing. Because of the complex structure of the biomimicking configuration area, we used smaller regular tetrahedral elements for this area, and other areas without biomimicking configuration use regular hexahedral elements. As before, we divided the grids of the

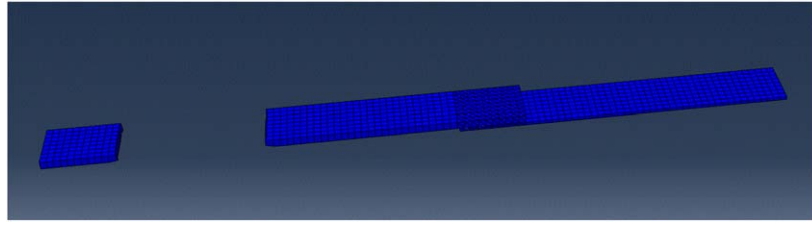


Figure 12. Schematic diagram of the fracture of the stainless-steel-and-plastic connector during the simulated tensile stress process.

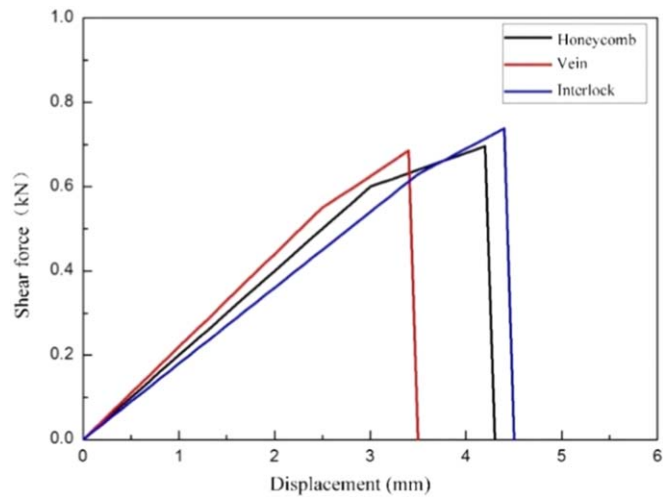


Figure 13. Force-displacement curve of the simulated the stretching of the stainless-steel-plastic connector.

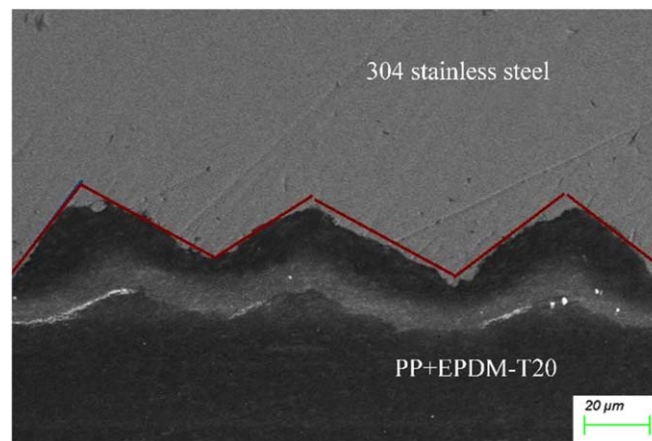
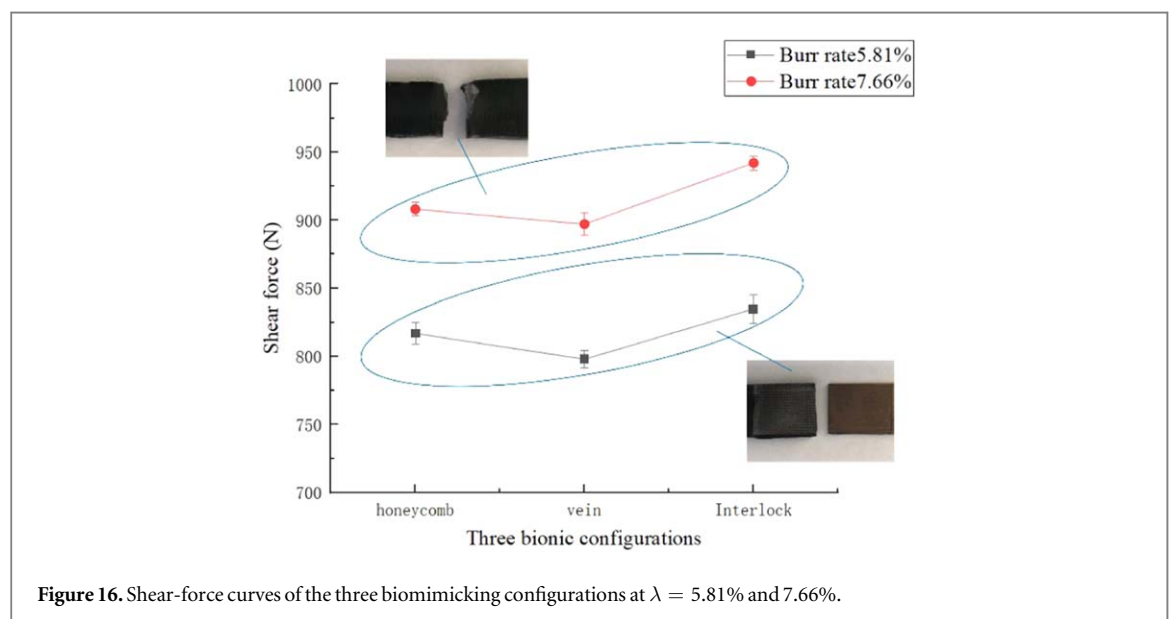
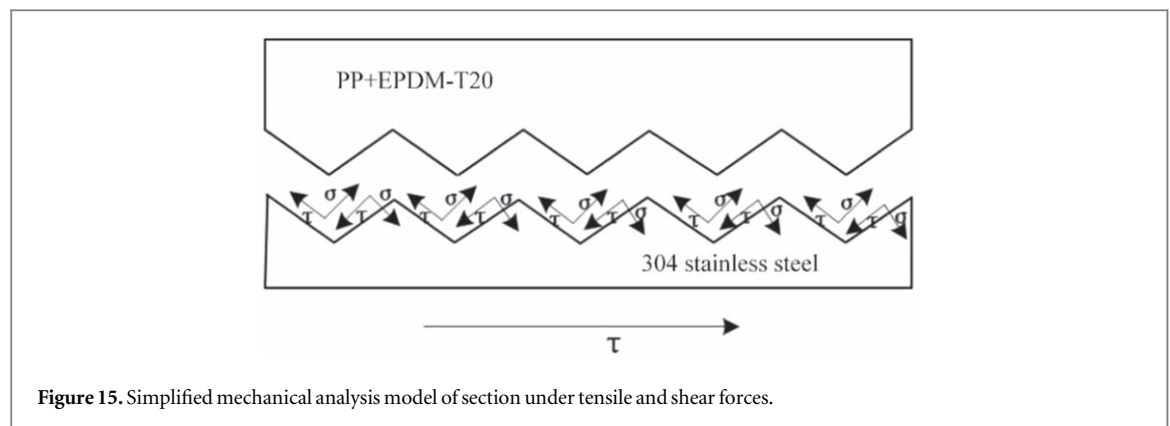


Figure 14. Scanning electron micrograph of the cross-section of the stainless-steel-plastic connection.

honeycomb configuration as an example (figure 10). The leaf veins and dragonfly head-and-neck hairs interlocking configurations are meshed in the same way.

4.3. Connection strength simulation of connectors

After constructing the finite element model, we simulated the displacement and force on the metal-plastic connector under a speed of 2 mm min^{-1} , and obtain the force-displacement curve and analyzed it to predict the best biomimicking configuration. In ABAQUS, the right end of the connector was restricted to translational and rotational degrees of freedom in the X, Y, and Z directions, the left end was restricted to the translation in the Y



and Z directions and rotation in the X, Y, and Z directions. The load was applied along the X direction. The horizontal force simulated the stress process of the tensile connector of the shear test machine (figure 11), which accurately predicted the influence of the biomimicking configuration on the connection strength.

The simulated tensile shear fracture of stainless-steel-plastic connection, is illustrated in figure 12. The shear force for the three configurations in the simulation process is depicted in figure 13. The force-displacement curve reveals that the vein configuration breaks at a displacement of 3.5 mm, under a shear force of 685 N. The honeycomb configuration breaks at 4.3 mm under 696 N. The dragonfly head-and-neck macrohair interlocking configuration breaks at 4.5 mm under 738 N. Based on the simulation data, we predict that the dragonfly configuration best promotes the strength of the connection between stainless steel and plastic.

5. Experimental analysis of metal-plastic connection strength

To verify the accuracy of the simulation results, two sets of tensile and shear tests with different burr rates were designed. The tests yielded the shear force values of the three biomimicking configurations, as well as their force-displacement curves. We also observed the microscopic surface morphology of the connecting surface and cross-section of the stainless-steel-plastic connector after the tensile and shear tests, analyzed the connection and the injection of molten plastic, and examined the best biomimicking structure that could improve the strength of the connection.

5.1. Mechanical analysis and experimental parameter design

The SEM image of the cross-section of the stainless-steel-plastic joint after the tensile shear test is displayed in figure 14. The shape of the joint is approximately a triangle, albeit irregular. This shape was simplified to render the processed model more regular for ease of calculation. Figure 15 depicts the simplified mechanical-analysis

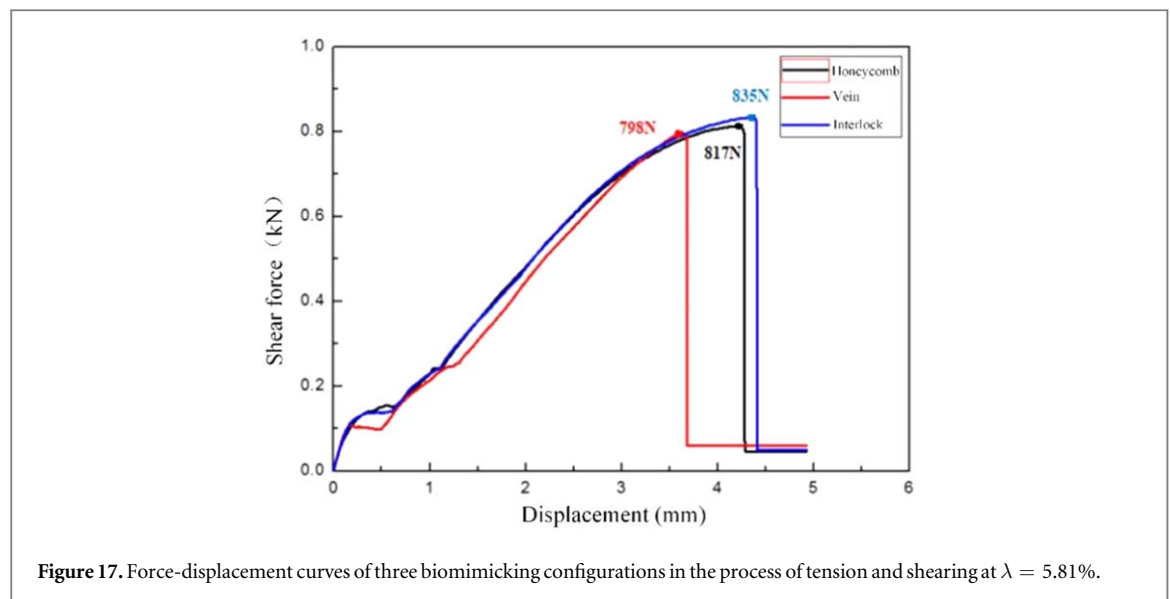


Figure 17. Force-displacement curves of three biomimicking configurations in the process of tension and shearing at $\lambda = 5.81\%$.

Table 4. Connection strength of different configurations and burr rates.

Number	Configuration	Burr rate (%)	Shear force and standard deviation (N)	Break location
1	Honeycomb	5.81	817 ± 7.94	Connection surface
2	vein	5.81	798 ± 6.56	Connection surface
3	Interlock	5.81	835 ± 10.44	Connection surface
4	Honeycomb	7.66	908 ± 5.20	Base material
5	Vein	7.66	897 ± 8.54	Base material
6	Interlock	7.66	942 ± 5.29	Base material

model of the stainless-steel-plastic joint. When the cross-section is a triangle, it bears both tensile and shear forces.

A force analysis was performed after obtaining the simplified mechanical model. The tensile force is represented as:

$$FN = [\sigma] \times S \quad (3)$$

where $[\sigma]$ is the allowable tensile stress. S is the cross-sectional area, $S = b \times h$, where b and h are the section's width and height, respectively.

The shear force is expressed as follows:

$$FS = [\tau] \times A \quad (4)$$

where $[\tau]$ is the allowable shear stress, and $A = 15 \times 20 \text{ mm}^2$.

With the honeycomb configuration as an example, the following formula is derived from equations (3) and (4):

$$F1 = [\tau_1]A + [\sigma_1]H1D \quad (5)$$

where F_1 is the load on the honeycomb configuration, $[\tau_1]$ is the allowable shear stress, and $[\sigma_1]$ is the allowable tensile stress. $A = 15 \times 20 \text{ mm}^2$. H_1 is the depth of the configuration, and D is the section width (15 mm).

The force equation of the leaf vein and dragonfly head-and-neck interlocking configurations were similarly derived from equations (3) and (4):

$$F2 = [\tau_2]A + [\sigma_2]H2D \quad (6)$$

$$F3 = [\tau_3]A + [\sigma_3]H3D \quad (7)$$

The single-factor control variable method was used during the experiment. To ensure the same coverage rate, three laser-processing areas with the same biomimicking configuration were designed. The marking times were the same in the process, thus ensuring that H_1 , H_2 , and H_3 in the formula were the same. Therefore, $F_1 = F_2 = F_3$ for the three configurations. Thus, we ensured that all the variables except the honeycomb, leaf vein, and dragonfly head-and-neck microhair interlocking configurations were consistent.

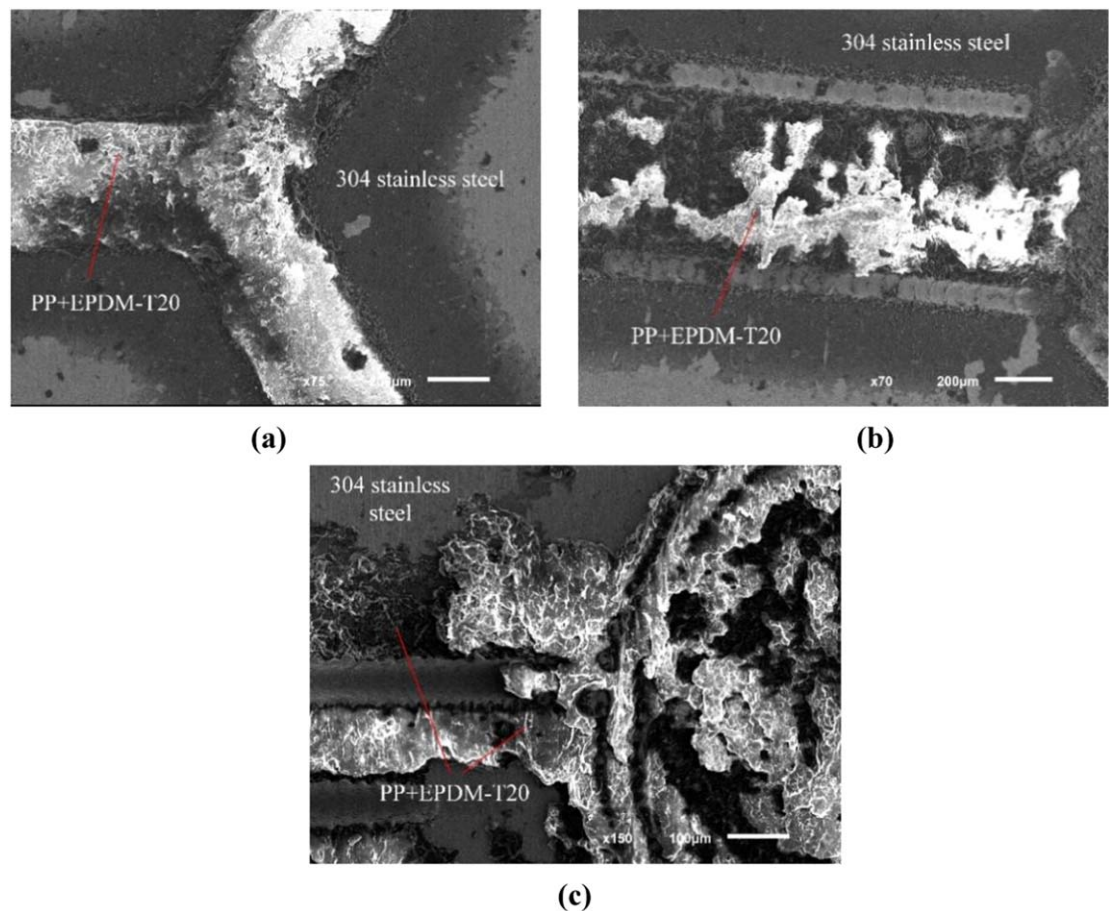


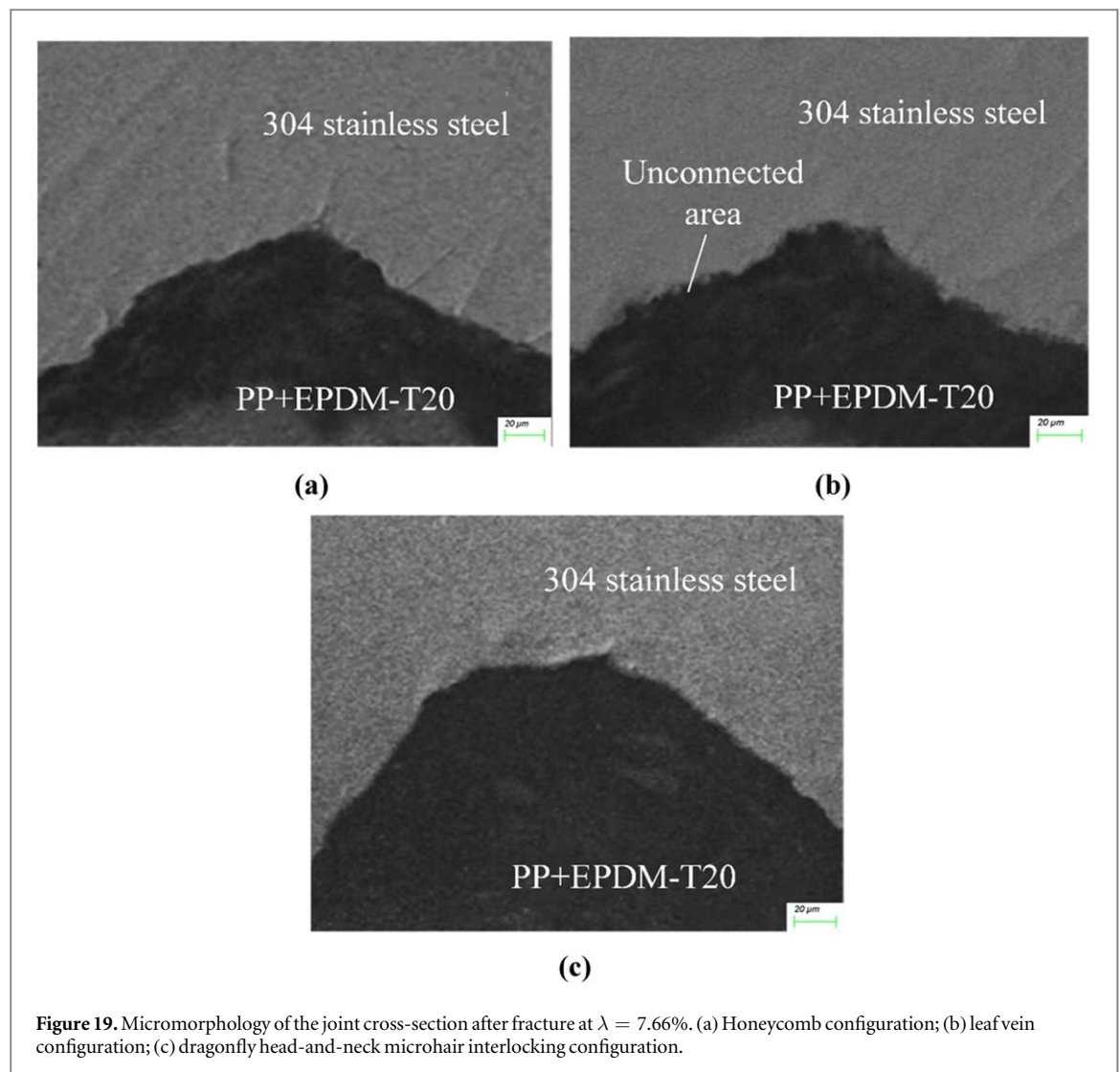
Figure 18. Surface micromorphology of the connector after fracture at a burr rate of 5.81%. (a) honeycomb configuration; (b) leaf vein configuration; (c) dragonfly head-and-neck microhair interlocking configuration.

5.2. The influence of bionic configuration on connection strength

Figure 16 illustrates the shear force curves of the three biomimicking configurations under different burr rates (λ). At $\lambda = 5.81\%$, the configurations failed at the connecting interface. At $\lambda = 7.66\%$, the shear force of the three configurations increased significantly, and they failed at the plastic base material. The performance of the configuration in the decreasing order of shear force is leaf vein < honeycomb < dragonfly head-and-neck microhair interlocking configurations. We concluded that all the three configurations improve the connection strength to varying degrees. At $\lambda = 7.66\%$, the dragonfly configuration has the highest shear force among the three. It also provides the strongest connection between the metal and plastic surfaces. The burr rate and connection strength of the three biomimicking connectors are listed in table 4.

Figure 17 illustrates the force–displacement curve obtained in the tensile test at $\lambda = 5.81\%$. It displays the same trend as the curve of the simulation results. However, numerical errors persist. Considering the stainless-steel specimen after laser treatment, these errors were caused by the formation of burrs on the surface, which were simplified for the simulation. The simulation results made provably reasonable and correct predictions based on the test results, which reflects the effectiveness of the simulation to a certain extent.

To further study the influence of the biomimicking configuration on the connection strength, we observed the surface micromorphology of the cross-section after fracture of the tensile–shear. Figure 18 depicts the SEM image of the biomimicking configuration on the stainless-steel surface after fracture of the connector when $\lambda = 5.81\%$. The distribution and adhesion of the molten plastic in the biomimicking configuration of the stainless-steel surface can be observed in the figure. As the plastic flows, the joint is broken at the connecting surface. The SEM image reveals that the molten plastic fills the entire laser-treated honeycomb configuration, albeit with a few bubbles and gaps (figure 18(a)). In the vein configuration, the molten plastic fills a small part of the laser-processed configuration (figure 18(b)). In the dragonfly head-and-neck microhair interlocking configuration, it fills the circular part. A large amount of the molten plastic is also attached to the surface of the untreated stainless steel. This effectively enhances the strength of the connection. However, the rectangular part of this configuration is not entirely filled (figure 18(c)). Combining the force–displacement curves of the three



configurations reveals that the vein configuration has the least amount of crevices filled with hot melt plastic, making the connection strength the weakest. Moreover, the fracture displacement of the tensile shear test machine for this configuration is also smaller than that for the other two. The main reason for the weak connection is the incomplete filling of the molten plastic. Further, the relatively large gap between the two materials hinders the formation of an effective mechanical lock. When $\lambda = 5.81\%$, the connecting piece breaks at the connecting surface in the tensile shear test, which is evidence that the burr rate does not promote effective locking with the biomimicking configuration between the molten plastic and the metal surface.

Figure 19 illustrates the SEM micrographs of the cross-sections of the three biomimicking connectors when $\lambda = 7.66\%$. Evidently, the two materials are connected, and the molten plastic has been injected into the biomimicking configuration under heat and pressure. Meanwhile, the connected samples broke at the plastic base material. As indicated in the SEM image, the plastic fills the entire configuration area at the cross-section of the honeycomb configuration, with virtually no gaps (figure 19(a)). At the cross-section of the vein configuration, the molten plastic does not fill the connecting area. The area has large gaps, as depicted in figure 19(b). At the cross-section of the dragonfly head-and-neck microhair interlocking configuration, the molten plastic fills the entire area. It is in close contact with the configuration, and the connection does not have gaps. At this point, the connection between the two materials is the strongest (figure 19(c)). The binding-force-displacement curve led to the conclusion that the dragonfly configuration is better than the others because it effectively promotes its structure. After the plastic is heated and melted to fill the biomimicking configuration of the stainless-steel surface, the connection strength between the two materials is further enhanced, yielding a shear force of $942 \pm 5.29 \text{ N}$, compared with the other two configurations. The microhair on the head-and-neck of a dragonfly use the principle of mechanical interlocking to achieve a better connection. When $\lambda = 7.66\%$, all the three connectors broke at the plastic base material. Thus, the connection strength of the three connectors at

this burr rate is greater than that of the material itself, and the interlocking configuration best enhances the connection strength between stainless steel and plastic.

6. Conclusions

The development of a biomimicking connector at the plastic–metal joint by laser processing significantly improved the connection strength between the two materials. Under heat and pressure, the molten plastic flows into the configuration on the stainless-steel surface, filling it and acting as an adhesive. Simultaneously, the burrs produced on the laser-processed surface form an effective mechanical lock, which further improves the connection strength of the two materials. The connection between stainless steel and plastic is the largest when the stainless-steel surface is etched with the interlocking configuration found between the head and neck microhairs on a dragonfly at a burr rate (λ) of 7.66% and a coverage rate (β) of 29.4%. The connector breaks at the plastic base material. When $\lambda = 5.81\%$, all the three types of connectors fail at the connection, and the interlocking configuration has the largest shear force of 835 N. When $\lambda = 7.66\%$, the connectors break at the plastic base material, and the dragonfly configuration still has the largest shear force of 942 N. This study will serve as a reference for the connecting of different thermoplastic polymer materials and stainless steel. It can be applied to the research of automobile lightweight to a greater extent.

Acknowledgments

This work was financially supported by Jilin Scientific and Technological Development Program (No. 20190302022GX).

Data availability statement

All data that support the findings of this study are included within the article (and any supplementary files).

ORCID iDs

Fengde Liu  <https://orcid.org/0000-0001-5894-861X>

References

- [1] Yeh R Y and Hsu R Q 2015 Application of porous oxide layer in plastic/metal direct adhesion by injection molding *Journal of Adhesion Science and Technology* **29** 1617–27
- [2] Korson C and Stratton D 2005 An integrated automotive roof module concept: plastic-metal hybrid and polyurethane composite technology *Proceedings of the 5th SPE Annual Automotive Composites Conference* (Troy, MI, Newport, CT.)
- [3] Lei D Q et al 2012 Experimental study of glass to metal seals for parabolic trough receivers *Renewable Energy* **48** 85–91
- [4] Zhao W, Barsun S, Ramani K et al 2001 Development of PMMA-precoating metal prostheses via injection molding: residual stresses *Journal of Biomedical Materials Research* **58** 456–62
- [5] Aglietti G S, Schwingshackl C W and Roberts S C 2007 Multifunctional structure technologies for satellite applications *The Shock and Vibration Digest* **39** 381–91
- [6] Sarlin E et al 2012 Vibration damping properties of steel/rubber/composite hybrid structures *Composite Structures* **94** 3327–35
- [7] Sarlin E et al 2014 Ageing of corrosion resistant steel/rubber/composite hybrid structures *Int. J. Adhes. Adhes.* **49** 26–32
- [8] Abbas M K G, Sakundarini N and Kong I 2019 Optimal selection for dissimilar materials using adhesive bonding and mechanical joining *Materials Science and Engineering* **469** 1–7
- [9] Li G et al 2012 Static strength of a composite butt joint configuration with different attachments *Compos. Struct.* **94** 1736–44
- [10] Fabrin P A, Hoikkanen M E and Vuorinen J E 2007 Adhesion of thermoplastic elastomer on surface treated aluminum by injection molding. *Polymer Engineering & Science* **47** 1187–91
- [11] Halder S, Sain T and Ghosh S 2017 A novel high symmetry interlocking micro-architecture design for polymer composites with improved mechanical properties *Int. J. Solids Struct.* **124** 161–75
- [12] Mandolino C, Lertora E and Gambaro C 2013 Effect of surface pretreatment on the performance of adhesive-bonded joints *Key Eng. Mater.* **554–557** 996–1006
- [13] Bagheri S and Guagliano M 2009 Review of shot peening processes to obtain nanocrystalline surfaces in metal alloys *Surf. Eng.* **25** 3–14
- [14] Annerfors C O and Petersson S 2007 *Nano molding technology on cosmetic aluminum parts in mobile phones* School of Mechanical Engineering Lund University
- [15] Chen L X, Liu Z Q and Shen Q 2018 Enhancing tribological performance by anodizing micro-textured surfaces with nano-MoS₂ coatings prepared on aluminum-silicon alloys *Tribol. Int.* **122** 84–95
- [16] Vilhena L M et al 2009 Surface texturing by pulsed Nd:YAG laser *Tribol. Int.* **42** 1496–504
- [17] Mao B et al 2020 Laser surface texturing and related techniques for enhancing tribological performance of engineering materials: a review *J. Manuf. Processes* **53** 153–73
- [18] Zhang X M, Yue T M and Man H C 1997 Enhancement of ceramic-to-metal adhesive bonding by excimer laser surface treatment *Mater. Lett.* **30** 327–32

- [19] Xu F *et al* 2019 Enhancement of the adhesion strength at the metal-plastic interface via the structures formed by laser scanning *Opt. Laser Technol.* **111** 635–43
- [20] Fan H Q, Liu S Y and Li Y Q 2020 The effect of laser scanning array structural on metal-plastic connection strength *Opt. Lasers Eng.* **133** 106107
- [21] Xing Y Q *et al* 2021 Formation of bionic surface textures composed by micro-channels using nanosecond laser on Si₃N₄-based ceramics. *Ceram. Int.* **47** 12768–79